Electronic supporting information

Synthesis of methanol by hydrogenolysis of biobased methyl formate using highly stable and active Cu-spinel catalysts in slurry and gas phase reactions

Vera Haagen[a], Jakob Iser[a], Markus Schörner[a], Dennis Weber[b], Tanja Franken[b], Peter Wasserscheid[a,b], Patrick Schühle[b]*

[a] V. Haagen, J. Iser, M. Schörner, Prof. Dr. P. Wasserscheid
Forschungszentrum Jülich, Helmholtz Institute for Renewable Energy Erlangen-Nürnberg, Cauerstraße 1, 91058 Erlangen, Germany

[b] D. Weber, Prof. Dr. Tanja Franken, Prof. Dr. P. Wasserscheid, Dr. Patrick Schühle
Friedrich-Alexander-Universität Erlangen-Nürnberg (FAU), Institute of Chemical Reaction Engineering, Egerlandstraße 3, 91058 Erlangen, Germany
*corresponding author: patrick.schuehle@fau.de

1. Experimental setup and flow-sheets

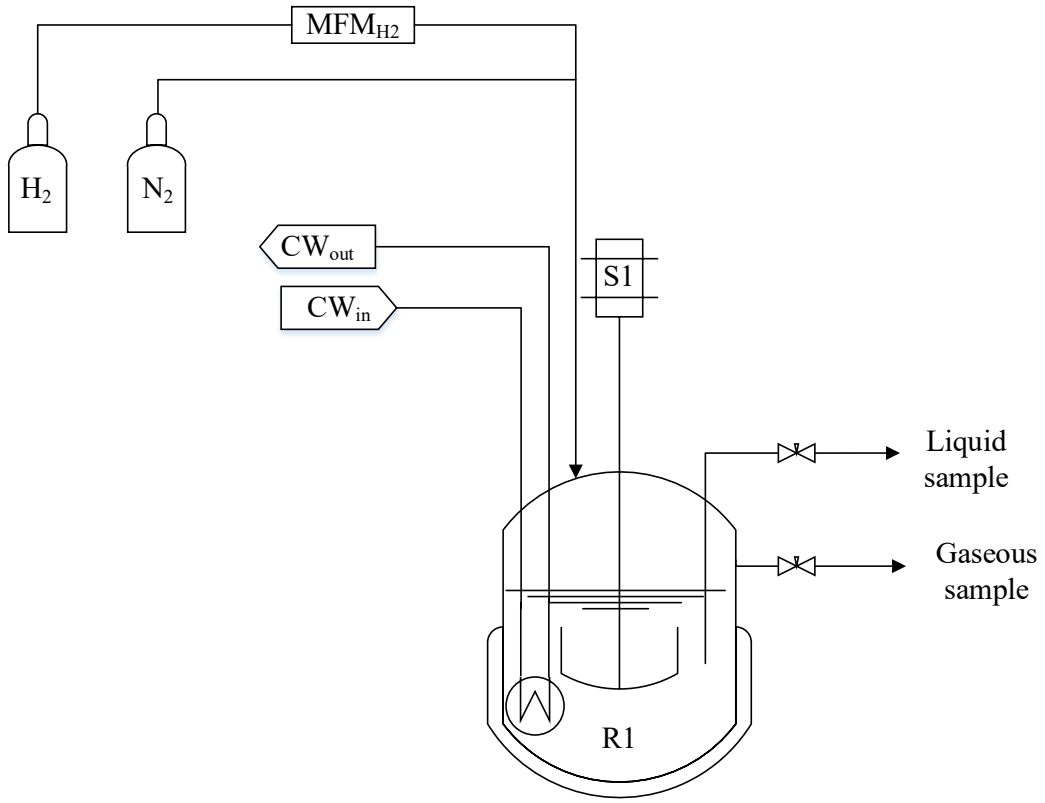

Figure S1: Slurry phase setup for MF hydrogenolysis, N_2 = pressurized nitrogen, H_2 = pressurized hydrogen, MFM = mass flow meter, R1 = hastelloy autoclave 300 mL, S1 = stirrer, CW = cooling water, OG = off gas.

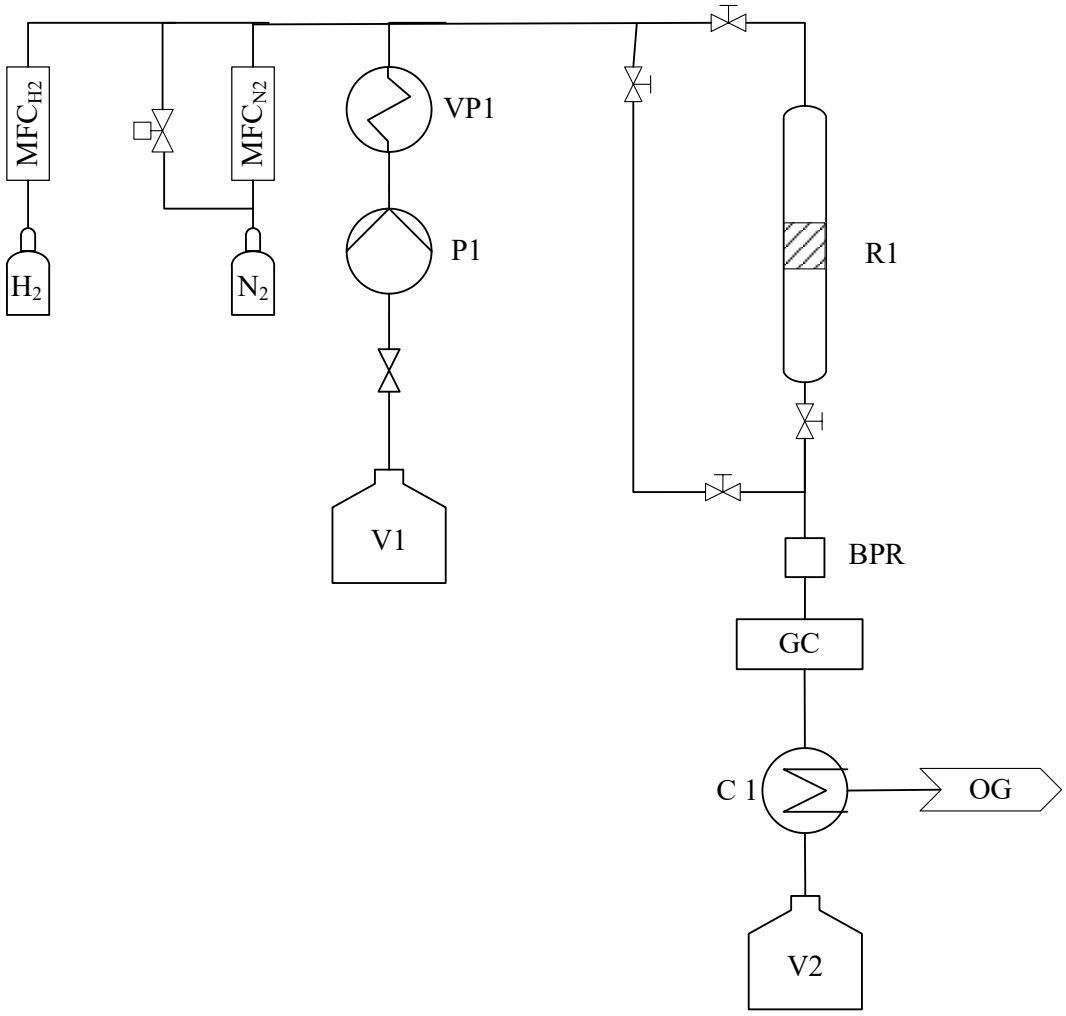

Figure S2: Continuous gas-phase setup for MF hydrogenolysis, N_2 / H_2= pressurized nitrogen / hydrogen, MFC = mass flow controller, V1 = storage vessel for MF, P1 = HPLC pump, VP1 = evaporator, R1 = fixed bed reactor with mounting for catalyst, BPR = back pressure regulator, GC = gas chromatograph, C1 = cooling, V2 = storage vessel for liquid products, OG = off gas.

2. Calculation details gas phase hydrogenolysis experiments

Determination of conversion and selectivity

For checking the mass balance, we used the ratio of MF to H_2. By determining the moles of each product and adding it stoichiometrically onto the reagent MF resp. H_2. Index 0 represents the inflow whereas index 1 stands for the product stream.

$$\dot{n}_{MF,0} = \dot{n}_{MF,1} + \dot{n}_{CO2,1} + \dot{n}_{CO,1} + \dot{n}_{DME,1} + 0.5 \cdot \dot{n}_{MeOH,1}$$

$$\dot{n}_{H2,0} = \dot{n}_{H2,1} + \dot{n}_{MeOH,1}$$

$$Molar\ ratio\ of\ H_2{:}MF = \frac{n_{H2,0}}{n_{MF,0}}$$

By comparing the molar ratio determined via above described manner with the actual inlet values (calculated via the mass flow of the reagents MF and H_2) the mass balance was in the range of 6 %.

The conversion of MF was determined according to:

$$X_{MF} = \frac{\dot{n}_{MF,0} - \dot{n}_{MF,1}}{\dot{n}_{MF,0}}$$

Selectivities were calculated based on a carbon basis. Therefore, the carbon containing massflow e.g. in CO_2 resp. DME was calculated as follows.

$$\dot{m}_{CO2,1} = \dot{n}_{CO2,1} \cdot \#C \cdot M_{CO2} = \dot{n}_{CO2,1} \cdot 1 \cdot 44 \frac{g}{mol}$$

$$\dot{m}_{DME,1} = \dot{n}_{DME,1} \cdot \#C \cdot M_{DME} = \dot{n}_{DME,1} \cdot 2 \cdot 46.07 \frac{g}{mol}$$

The selectivity using the example of DME was determined according to

$$S_{DME} = \frac{\dot{m}_{DME,1}}{\dot{m}_{MF,1} - \dot{m}_{MF,0}}$$

The productivity based on the active copper surface was determined as follows:

$$P_{active} = \frac{\dot{m}_{MeOH,1}}{m_{Cat} \cdot S_{RFC}}$$

Determination of apparent activation energy $E_{A,eff}$

R_{eff} was determined from measurement data as follows:

$$r_{eff} = \frac{\dot{n}_{MeOH,1}}{V_{Catalyst}}$$

For the determination of the apparent activation energy, the kinetic potency approach was linearized assuming constant concentrations of reagents due to low conversions (X_{MF} < 12 %):

$$r_{eff} = k_0 \cdot e^{\frac{-E_{A,eff}}{R \cdot T}} \cdot p_{MF}^{a} p_{H2}^{b} = K \cdot e^{\frac{-E_{A,eff}}{R \cdot T}}$$

$$\ln\left(r_{eff}\right) = K - \frac{E_{A,eff}}{R \cdot T}$$

By plotting the above mentioned linear equation, the apparent activation energy $E_{A,\,eff}$ can be determined according to the slope of the graph.

Determination of the reaction orders n_{MF} and n_{H2}

For the determination of the reaction orders, the kinetic potency approach was linearized assuming constant temperature. Furthermore, in experiments for the determination of n_{MF} H_2 was used in excess to guarantee no limiting effects of the latter. The same was applied vice versa for n_{H2}.

By linearizing the kinetic potency approach, the slope of the log r_{eff} vs log (p_{MF}) resp. log (p_{H2}) plot gives the order of the MF hydrogenolysis reaction with respect to MF (a) resp. H_2 (b) partial pressure.

$$r_{eff} = k_0 \cdot e^{\frac{-E_{A,eff}}{R \cdot T}} \cdot p_{MF}^{a} p_{H2}^{b}$$

$$r_{eff} = K \cdot p_{MF}^{a}$$

$$\log r_{eff} = \log K + a \cdot \log p_{MF}$$

3. Reproduction experiments using CuO/ZnO in slurry phase

Table S1: Conversion and selectivity of reproduction experiments in slurry phase using CuO/ZnO catalyst with absolute and relative standard deviation, reaction conditions: T = 175 °C, p_{H2} = 45 bar_g (p_{total} = 80 bar_g), t = 1.5 h, m_{MF}:m_{Cu} = 48.3 g g^{-1}, m_{MF} = 120 g, 1000 rpm.

Experiment	**X_{MF} / %**	**S_{MeOH} / %**	**S_{CO} / %**	**S_{CO2} / %**
1	31.8	89.6	7.6	1.8
2	26.3	88.8	8.2	1.9
3	24.8	88.9	6.9	2.0
Absolute standard deviation / %	3.0	0.4	0.5	0.1
Relative standard deviation / %	10.9	0.5	7.2	5.3

4. Catalyst characterization results

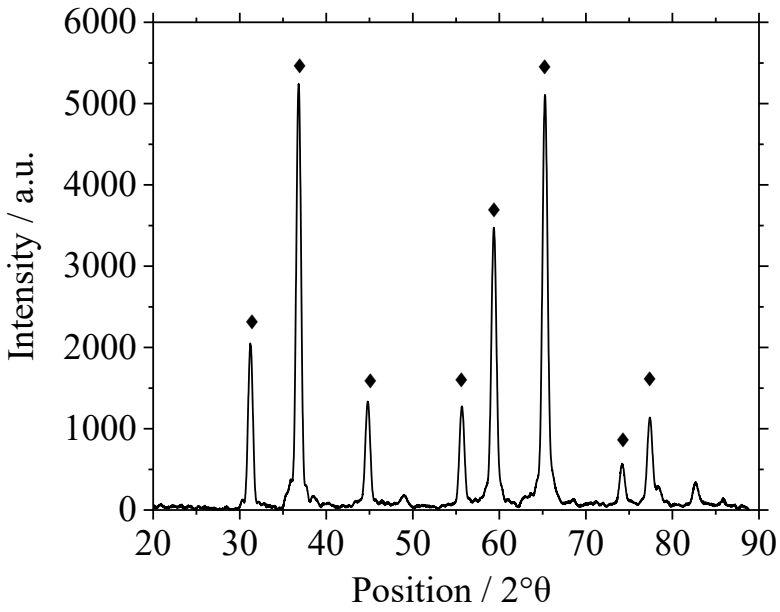

Figure S3: XRD Pattern of $Cu_{0.9}Al_2O_4$. Characteristic reflexes for $Cu_{0.9}Al_2O_4$ are marked with ◆ [1].

Figure S4: Filtrates of CuO/ZnO-B experiment. The blue colour is typical for copper formate species.

Figure S5: Filtrates of CuO/Cr_2O_3-B experiment. The blue colour is typical for copper formate species.

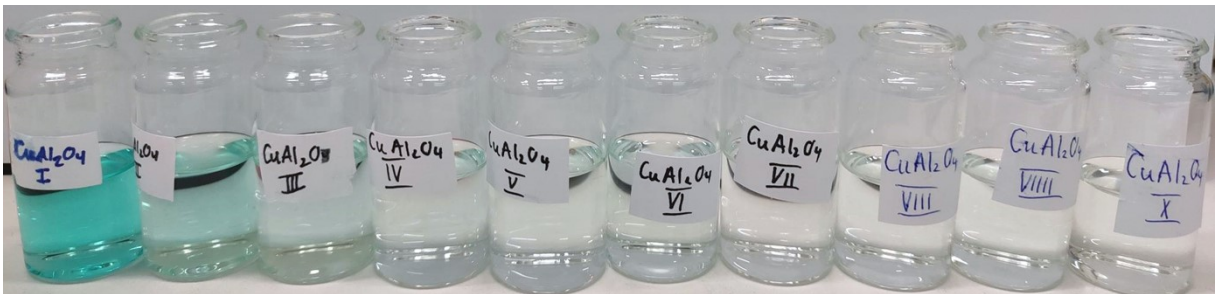

Figure S6: Filtrates of $Cu_{0.9}Al_2O_4$ experiment. The blue coloration in filtrate I is caused by synthesis-related traces of CuO, which react with FA to copper formate. After complete dissolution of the CuO-traces, no coloration of the filtrates was observed.

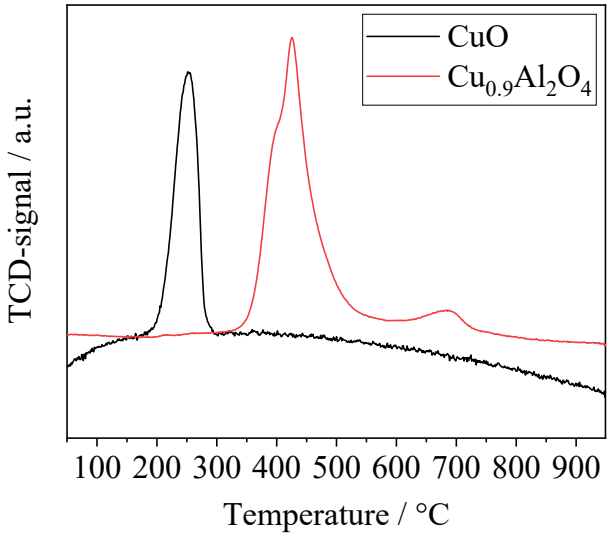

Figure S7: TPR spectra of CuO and $Cu_{0,9}Al_2O_4$, reaction conditions: 20 % H_2 in argon, 5 K min^{-1}.

5. Influence of gaseous formic acid on Cu-catalysts

Experimental setup

To investigate the influence of vaporized FA on the stability of Cu-catalysts a glass setup was used (see Figure S 8). An aqueous solution of FA (n_{H2O}:n_{MF} = 19 mol mol^{-1}) was added into a glass flask and heated to 80 °C under continuous stirring. Using a constant flow of N_2 (20 ml_N min^{-1}) the solution was stripped out of the flask into a heated column (200 °C) where the catalyst (2 g) was fixed on a glass frit. On top of the column the liquid products were condensed and collected.

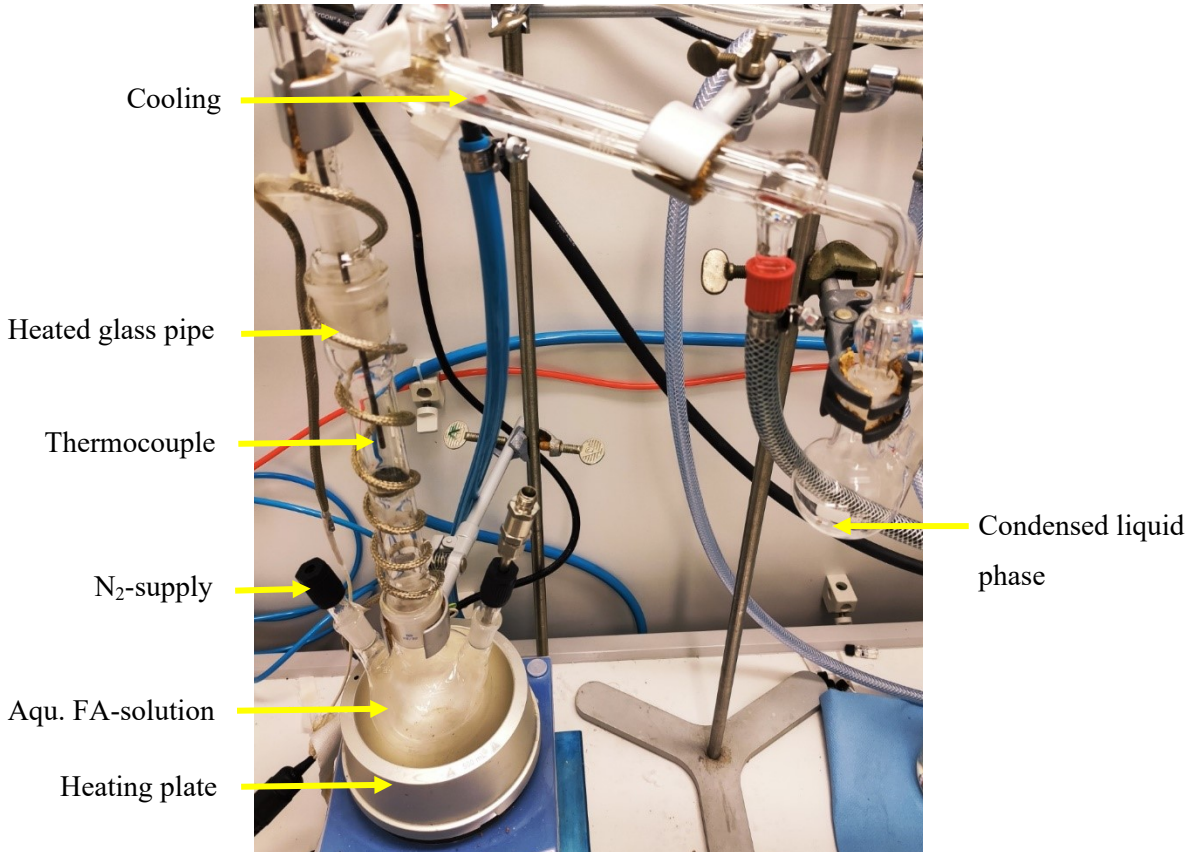

Figure S 8: Glass setup for the investigation of influence of gaseous FA on catalysts.

In this setup, we investigated the catalysts applying the following two scenarios and the results were compared to the usage of the fresh catalyst as reference: i) contact of the catalyst with FA-enriched nitrogen for 6 h at 200 °C; ii) contact of the catalyst with FA-enriched nitrogen for 1 h at 200 °C followed by condensation in the catalyst material (catalyst heating shut-down for 1 h) and subsequent reheating to 200 °C for 1 h.

After both scenarios the catalyst was flushed with pure N_2 at 200 °C for 3 h. Finally, the setup was cooled down under N_2 flow. After the treatment, the catalysts were analysed using ICP, BET and RFC.

Experimental results

MF hydrogenolysis is often performed in gas phase reactor concepts. Working in gas phase could be advantageous, since contact of Cu with gaseous FA might not lead to metal leaching. Nevertheless, a possible condensation of FA, e.g. during start-up and shut-down phases cannot be excluded. Furthermore, renewable H_2 provision is time depending, suggesting a dynamic operation of MF hydrogenolysis [2]. In a dynamic operation mode, however, local condensation of FA becomes very likely due to a time dependent change of reaction temperatures. To examine the stability of the Cu-catalysts in a continuous gas phase process, we additionally investigated the influence of gaseous FA on the Cu-catalysts in a glass setup according to the procedure described in experimental setup section. The results are shown in Table S2.

Table S2: Comparison of CuO/ZnO, CuO/Cr_2O_3, $Cu_{0.9}Al_2O_4$ in the fresh state, after treatment with gaseous FA for 6 h (FA evaporation) as well as after catalyst treatment with gaseous FA for 1 h, condensation of FA for 1 h and subsequent heating (FA condensation), reaction conditions: T = 200 °C, p = 1 atm, $\dot{V}_{N2}$ = 20 $ml_N\,min^{-}$

	Scenario	**S_{RFC} / $m_{Cu}^2\,g^{-1}$**
CuO/ZnO	fresh	44
	FA evaporation	34
	FA condensation	16
CuO/Cr_2O_3	fresh	15
	FA evaporation	10
	FA condensation	7
$Cu_{0.9}Al_2O_4$*	fresh	1.1
	FA evaporation	1.2
	FA condensation	1.2

$Cu_{0.9}Al_2O_4$: Usage of same catalyst batch as in scenario A and C*

By comparing results from the fresh catalysts with those treated with evaporated FA, the influence of gaseous formic acid was examined. We observed a slight decrease of the active copper surface area from 44 $m_{Cu}^2\,g^{-1}$ to 34 $m_{Cu}^2\,g^{-1}$ using CuO/ZnO and from 15 to 10 $m_{Cu}^2\,g^{-1}$ for CuO/Cr_2O_3. Obviously, FA corrosion leads to a change in the surface properties for CuO/ZnO and CuO/Cr_2O_3 also in gas phase. In contrast, no reduction in active copper surface area is observed after the gas phase FA-treatment for $Cu_{0.9}Al_2O_4$.

The influence of FA condensation on the Cu-catalysts can be derived from a comparison of the fresh catalyst with the same material after forced FA condensation (FA condensation results in Table S2). The results clearly show, that periods of FA condensation have a negative influence on the active copper surface area. In the two experiments with CuO/ZnO and CuO/Cr_2O_3, a characteristic blue coloration of the inert glass wool, which was placed underneath the catalyst, was observed during condensation

(Figure S9-10). This hints for the formation and leaching of $Cu(HCOO)_2$. With increasing temperature, the instable $Cu(HCOO)_2$-species decompose and elemental copper remains. In-line with this interpretation, ICP-OES measurements of deposits that were found on the surface of the used glass tube after the experiment (Figure S9-10) consisted mainly of copper. The treatment with condensed FA leads to a stronger decrease in active copper surface for CuO/ZnO and CuO/Cr_2O_3 compared to the previously described results with a gaseous FA treatment. Conversely, using the $Cu_{0.9}Al_2O_4$, neither a change in catalysts properties nor the formation of copper deposits (see Figure S11) after FA condensation on the reactor surface was observed. These experiments show that for a technical application scenario the contamination of the downstream part of hydrogenolysis plant with leached Cu- and Cr-species has to be expected if CuO/ZnO and CuO/Cr_2O_3 catalysts are applied and FA impurities are present. In contrast, the $Cu_{0.9}Al_2O_4$ shows high stability against gaseous and condensed FA.

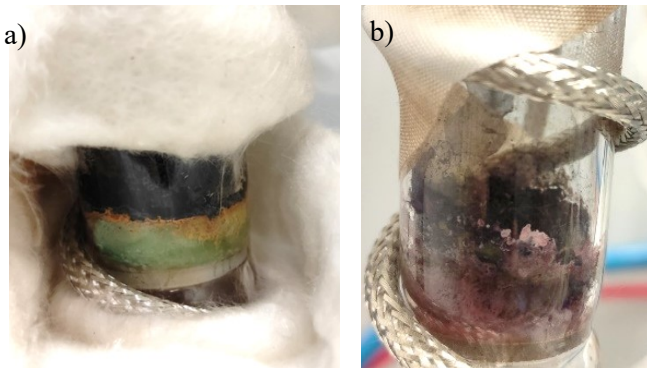

Figure S9: a) Photography of experiment CuO/ZnO-E during condensation of a FA-H_2O mixture (n_{H2O}:n_{MF} = 19 mol mol^{-1}). The green-blue coloration is typical for copper formate species, b) Photography of experiment CuO/ZnO-E after condensation and heating at 200 °C for 3 h. Copper deposition can be observed on the glass wall.

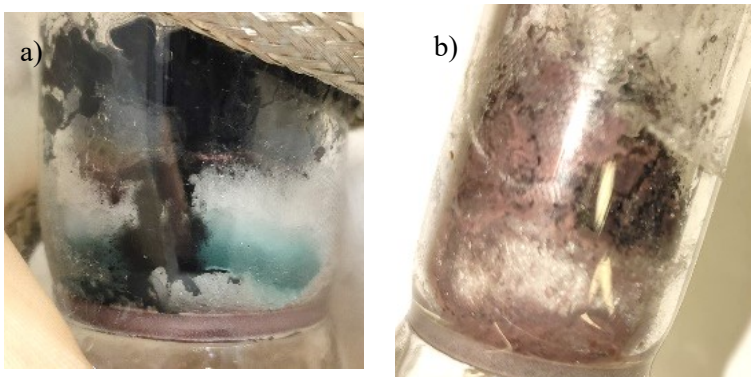

Figure S10: a) Photography of experiment CuO/Cr_2O_3-E during condensation of a FA-H_2O mixture (n_{H2O}:n_{MF} = 19 mol mol^{-1}). The green-blue coloration is typical for copper formate species, b) Photography of experiment CuO/Cr_2O_3-E after condensation and heating at 200 °C for 3 h. Copper deposition can be observed on the glass wall.

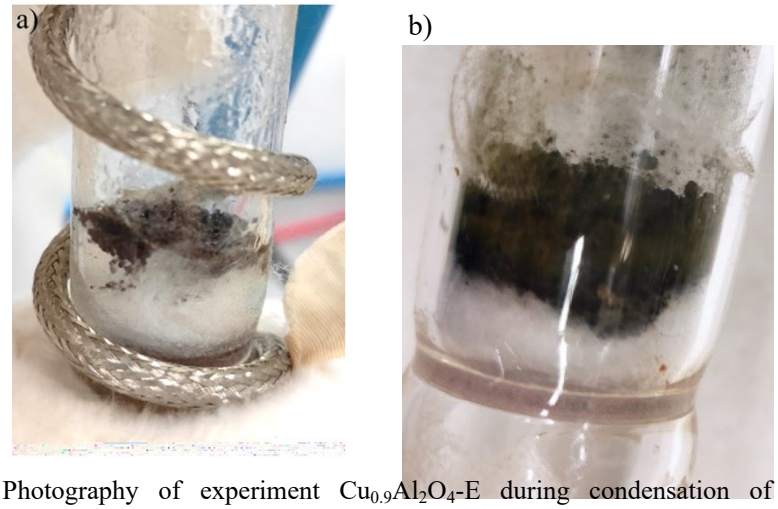

Figure S11: a) Photography of experiment $Cu_{0.9}Al_2O_4$-E during condensation of a FA-H_2O mixture (n_{H2O}:n_{MF} = 19 mol mol^{-1}). No coloration of glass wool is observed. b) Photography of experiment $Cu_{0.9}Al_2O_4$-E after condensation and heating at 200 °C for 3 h. No copper deposition on the glass surface was observed.

6. Influence of water on hydrogenolysis of methyl formate in gas phase using $Cu_{0.9}Al_2O_4$

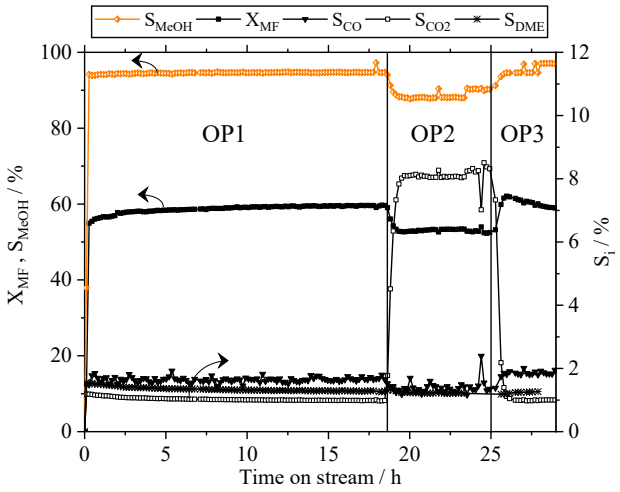

Figure S 12: Conversion and selectivity depending on reaction time for $Cu_{0,9}Al_2O_4$-catalyst, OP1 and OP3: usage of pure methyl formate as substrate, OP2: usage of a H_2O-methyl formate-mixture (1.5 w.-% H_2O) as substrate, reaction conditions: T = 218 °C, p = 10 bar_g, , n_{H2} n_{MF}^{-1} = 5.6 mol mol^{-1}, V_{total} = 704 ml_N min^{-1}, $m_{Cat.}$ = 0.5 g.

According to Figure S12 the Cu spinel catalyst shows a constant performance within the first 17 h (OP1). By replacing pure methyl formate by a methyl formate-water-mixture a increase in selectivity towards CO_2 (from 1% to appr. 8%) was observed (OP2). Simultaneously, the MeOH selectivity and methyl formate conversion decreased in OP2. The increase of CO_2-selectivity can be explained by the hydrolysis of methyl formate in the presence of water producing MeOH and FA. The latter is converted to CO_2 and H_2. Via balancing, it could be confirmed that the amount of H_2O added in BP2 corresponds in good agreement to the increase of CO_2 in BP2. However, by replacing the water-methyl formate-mixture with pure MF in OP3, an increase in conversion and methanol selectivity to comparable values as in OP1 is reached again. Consequently, the decrease in methanol selectivity and conversion is reversible, showing that theCu spinel catalyst is stable also in the presence of water.

7. Comparison of CuO/ZnO, CuO/Cr_2O_3 and $Cu_{0.9}Al_2O_4$ in continuous gas phase setup

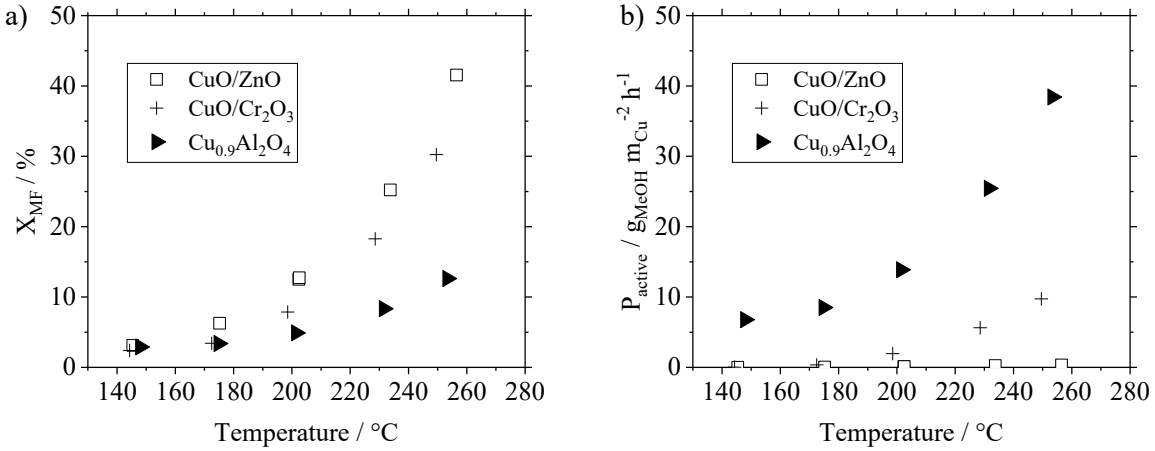

Figure S13: a) Conversion and b) productivity based on active copper surface area for CuO/ZnO, CuO/Cr_2O_3 and $Cu_{0.9}Al_2O_4$ in continuous gas phase setup, reaction conditions: T = 145-260 °C, p = 10 bar_g, V_{total} = 704 ml_N min^{-1}, n_{H2}:n_{MF} = 5.8, $m_{cat.}$ = 0.5 g (CuO/ZnO), 0.03 g (CuO/Cr_2O_3), 0.05 g ($Cu_{0.9}Al_2O_4$).

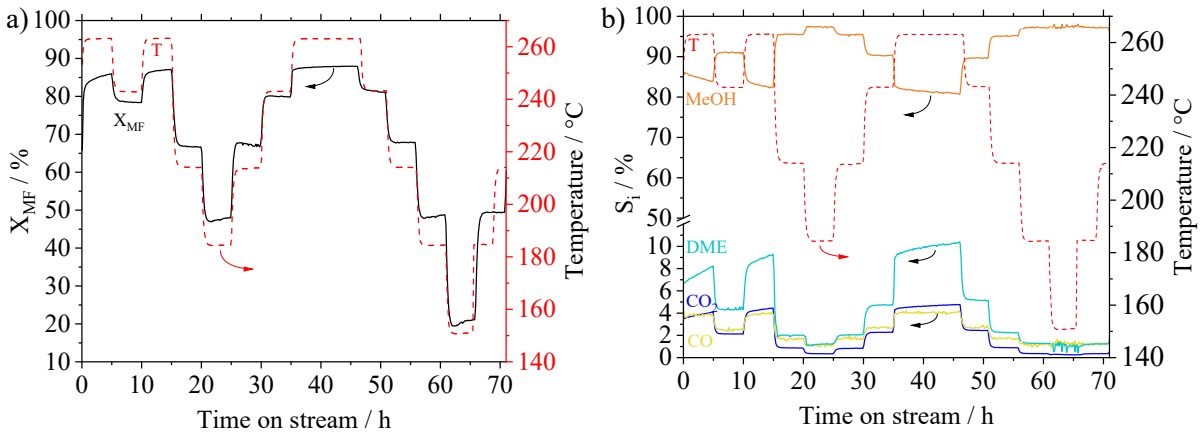

Figure S14: Conversion and b) selectivity over time for $Cu_{0.9}Al_2O_4$ at various reaction temperatures, reaction conditions: T = 150-260 °C, p = 10 bar_g, V_{total} = 704 ml_N min^{-1}, n_{H2}:n_{MF} = 5.8, $m_{cat.}$ = 0.5 g.

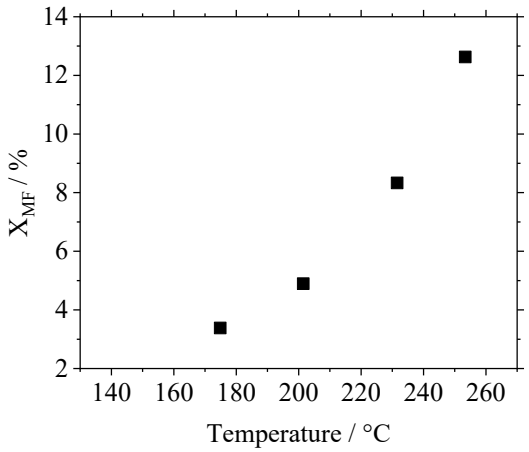

Figure S15: Conversion depending on the temperature for $Cu_{0.9}Al_2O_4$, reaction conditions: T = 175-260 °C, p = 10 bar_g, V_{total} = 704 $ml_N\,min^{-1}$, n_{H2}:n_{MF} = 5.8, $m_{cat.}$ = 0.05 g.

8. Determination of apparent activation energies for CuO/ZnO and CuO/Cr_2O_3

CuO/ZnO

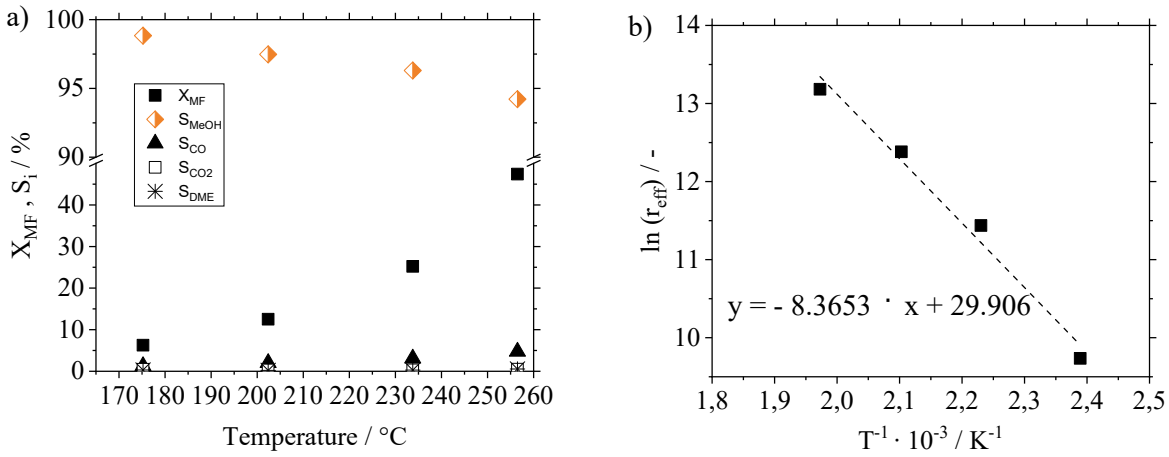

Figure S16: a) Conversion and selectivity depending on temperature for CuO/ZnO catalyst and b) arrhenius plot for the determination of apparent activation energy, reaction conditions: T = 175-255 °C, p = 10 bar_g, V_{total} = 704 $ml_N\,min^{-1}$, n_{H2}:n_{MF} = 5.8, $m_{cat.}$ = 0.1 g.

CuO/Cr_2O_3

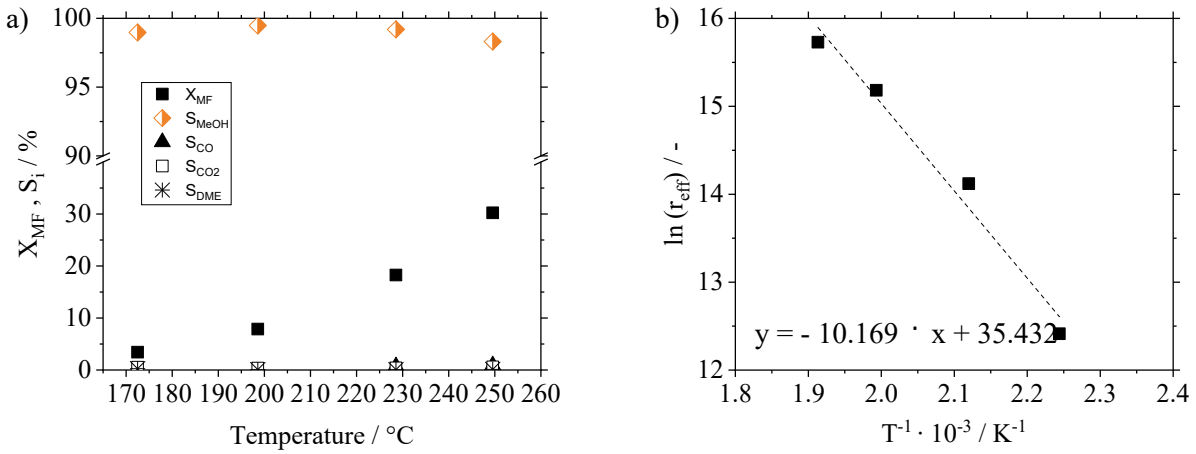

Figure S17: a) Conversion and selectivity depending on temperature for CuO/Cr_2O_3 catalyst and b) arrhenius plot for the determination of apparent activation energy, reaction conditions: T = 172-250 °C, p = 10 bar_g, V_{total} = 704 $ml_N\,min^{-1}$, n_{H2}:n_{MF} = 5.8, $m_{cat.}$ = 0.03 g.

9. Determination of reaction orders for CuO/ZnO, CuO/Cr_2O_3 and $Cu_{0.9}Al_2O_4$

$Cu_{0.9}Al_2O_4$

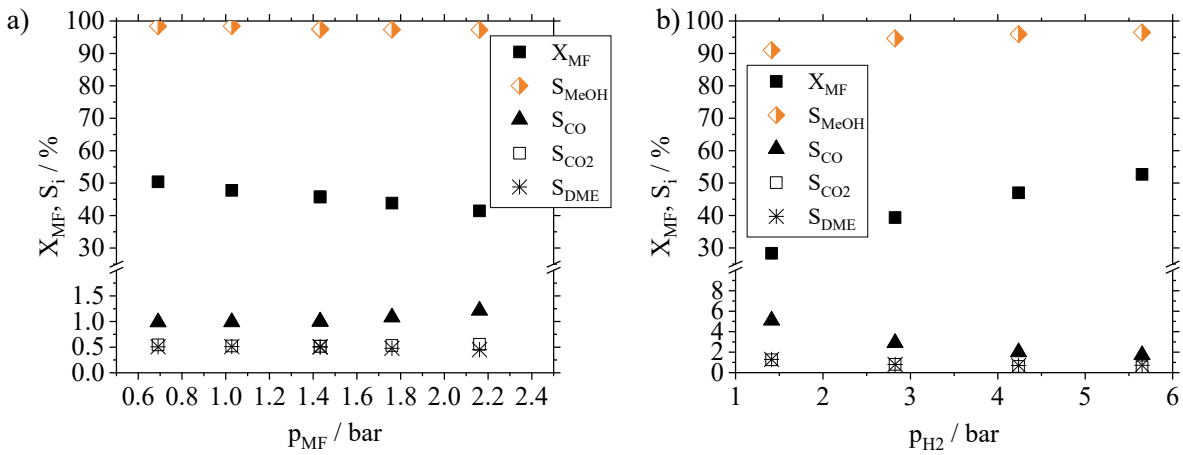

Figure S18: Conversion depending on partial pressure of a) MF, p_{MF} = 0.69-2.16 bar, p_{H2} = 8.5 bar and b) H_2, p_{MF} = 1.44 bar, p_{H2} = 1.41-5.65 bar, reaction conditions: p = 10 bar_g, T = 210 °C, $m_{cat.}$ = 0.5 g, $Cu_{0.9}Al_2O_4$.

CuO/ZnO

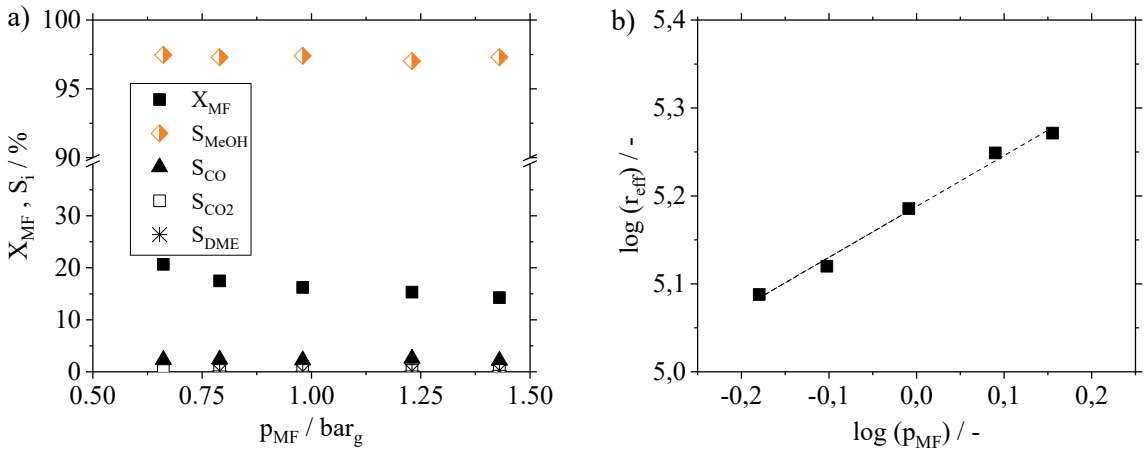

Figure S19: a) Conversion and selectivity depending on partial pressure of MF and b) Linearized potency approach for determination of n_{MF}, reaction conditions: T = 208 °C, p = 10 bar_g, p_{MF} = 0.7-2.2 bar, p_{H2} = 8.4 bar, $m_{cat.}$ = 0.5 g, V_{total} = 704 $ml_N\,min^{-1}$, CuO/ZnO.

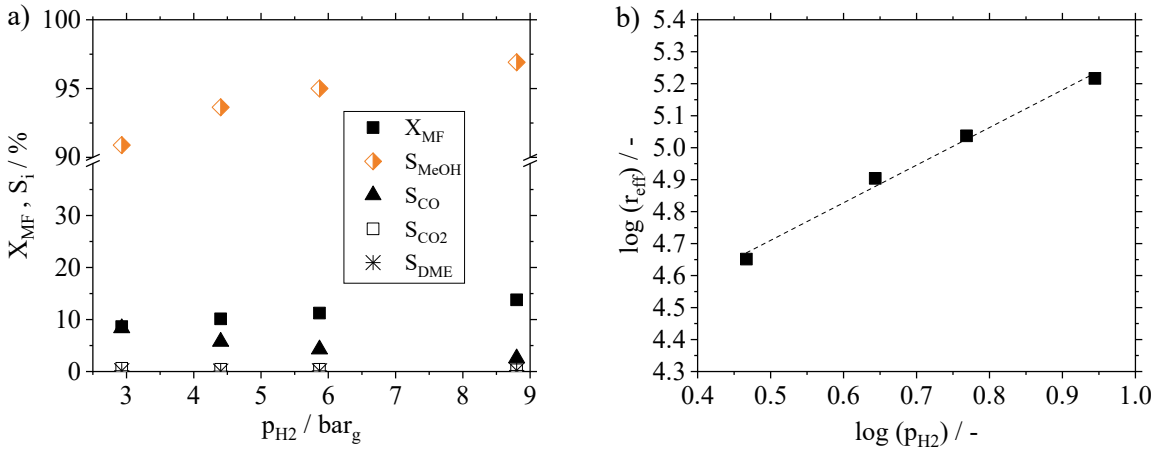

Figure S20: a) Conversion and selectivity depending on partial pressure of H_2 and b) Linearized potency approach for determination of n_{H2}, reaction conditions: T = 200 °C, p = 10 bar_g, p_{MF} = 1.49 bar, p_{H2} = 2.9-8.8 bar, $m_{cat.}$ = 0.5 g, V_{total} = 704 ml_N min^{-1}, CuO/ZnO.

CuO/Cr_2O_3

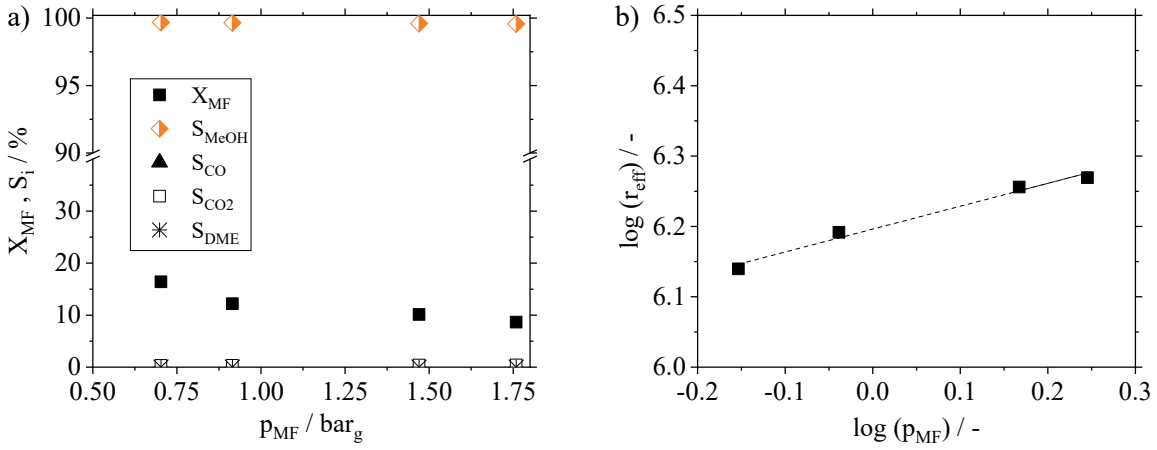

Figure S21: a) Conversion and selectivity depending on partial pressure of MF and b) Linearized potency approach for determination of n_{MF}, reaction conditions: T = 200 °C, p = 10 bar_g, p_{MF} = 0.7-1.8 bar, p_{H2} = 8.8 bar, $m_{cat.}$ = 0.03 g, V_{total} = 704 ml_N min^{-1}, CuO/Cr_2O_3.

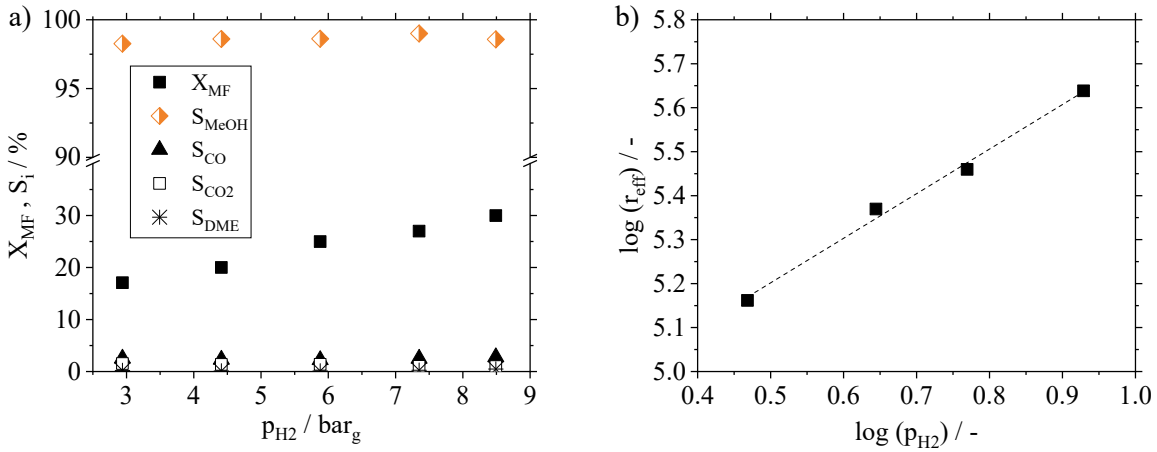

Figure S22: a) Conversion and selectivity depending on partial pressure of H_2 and b) Linearized potency approach for determination of n_{H2}, reaction conditions: T = 260 °C, p = 10 bar_g, p_{MF} = 1.49 bar, p_{H2} = 2.9-8.8 bar, $m_{cat.}$ = 0.03 g, V_{total} = 704 ml_N min^{-1}, CuO/Cr_2O_3.

10. References

[1] T. Tangcharoen, J. T-Thienprasert and C. Kongmark, *Journal of Advanced Ceramics*, 2019, 8, 3, 352-366.

[2] L. M. Gandia, G. Arzamendi, P. M. Dieguez, *Renewable Hydrogen Technologies: Production, Purification, Storage, Applications and Safety*, Elsevier Science, 2013.